Cavitation in an orifice flow

S. Dabiri and W. A. Sirignano
Department of Mechanical and Aerospace Engineering, University of California, Irvine, California 92697-3975, USA

D. D. Joseph
Department of Aerospace Engineering and Mechanics, University of Minnesota, Minneapolis, Minnesota 55455, USA

(Received 3 February 2007; accepted 24 May 2007; published online 30 July 2007)

The purpose of this study is to identify the potential locations for cavitation induced by total stress on the flow of a liquid through an orifice of an atomizer. A numerical simulation of two-phase incompressible flow is conducted in an axisymmetric geometry of the orifice for Reynolds numbers between 100 and 2000. The orifice has a rounded upstream corner and a sharp downstream corner with length-to-diameter ratio between 0.1 and 5. The total stress including viscous stress and pressure has been calculated in the flow field and, from there, the maximum principal stress is found. The total-stress criterion for cavitation is applied to find the regions where cavitation is likely to occur and compared with those of the traditional pressure criterion. Results show that the viscous stress has significant effects on cavitation. The effect of geometry and occurrence of hydraulic flip in the orifice on the total stress are studied. The Navier-Stokes equations are solved numerically using a finite-volume method and a boundary-fitted orthogonal grid that comes from the streamlines and potential lines of an axisymmetric equipotential flow in the same geometry. A level-set formulation is used to track the interface and model the surface tension. © *2007 American Institute of Physics*. [DOI: 10.1063/1.2750655]

I. INTRODUCTION

High-pressure atomizers and spray generators are of great interest in industry and have many applications such as combustors, drying systems, and agricultural sprays.

Recent experimental studies by Tamaki *et al.*[1,2] and Hiroyasu[3] show that the occurrence of cavitation inside the nozzle makes a substantial contribution to the breakup of the exiting liquid jet. Figure 1 shows a schematic of their experiment. The collapse of cavity bubbles can increase the disturbances in the flow leading to a faster breakup of the jet. Even with high-pressure drops, the main flow of liquid jet does not atomize greatly when disturbances caused by cavitation are not present.

In a different experiment, Otendal *et al.*[4] studied the breakup of high-speed liquid jet in vacuum, where the pressure is lower than the vapor pressure. By an appropriate design of the nozzle, they avoided the cavitation-induced instabilities inside the nozzle. By decreasing the air pressure below the vapor pressure, they observed a bursting phenomena due to cavitation in the free jet.

Bunnell *et al.*[5] studied the unsteady cavitating flow in a slot and found that partially cavitated slots show a periodic oscillation with Strouhal number near unity based on orifice length and Bernoulli velocity.

Tafreshi and Pourdeyhimi[6] carried out a numerical simulation on cavitation and hydraulic flip inside hydroentangling nozzles. They showed that under certain conditions cavity extends to the nozzle outlet and results in hydraulic flip. When hydraulic flip occurs, cavitation vanishes due to the fact that downstream air moves upstream into the nozzle. This leads into the elongation of the jet breakup length. Ahn *et al.*[7] experimentally studied the effects of cavitation and hydraulic flip on the breakup of the liquid jet injected perpendicularly into subsonic crossflow. They showed that cavitation results in shortening the liquid column breakup length. They observed a smaller breakup length in the hydraulic flip due to the fact that the jet diameter was smaller than the orifice diameter. Jung *et al.*[8] considered the breakup characteristics of liquid sheets formed by a like-doublet injection. They found that liquid-jet turbulence delays sheet breakup and shortens wavelengths of both ligaments and sheets. Ganippa *et al.*[9] considered the cavitation growth in the nozzle as they increased the flow rate. First, traveling bubbles are created. These bubbles are detached from the wall and move with the stream. By increasing the flow rate, the unsteady cloud of cavitation is observed. Further increasing in the flow rate caused the nonsymmetrical distribution of cavitation within the nozzle and its extension to the nozzle exit. More atomization occurs at the side with stronger cavitation.

The nucleation sites, where cavitation begins, are of two types. In case of homogeneous nucleation, these sites are temporary, microscopic voids that are results of the thermal motions within the liquid. However, in practical situations the rupture occurs at the boundary between the liquid and solid wall of container, or between liquid and small solid particles suspended in the liquid. In these cases heterogeneous nucleation occurs at the solid/gas interface.[10]

In the traditional criterion of cavitation, cavitation occurs when the pressure drops below the breaking strength of liquid, which we call critical pressure or critical stress, and in an ideal case is the vapor pressure at local temperature.

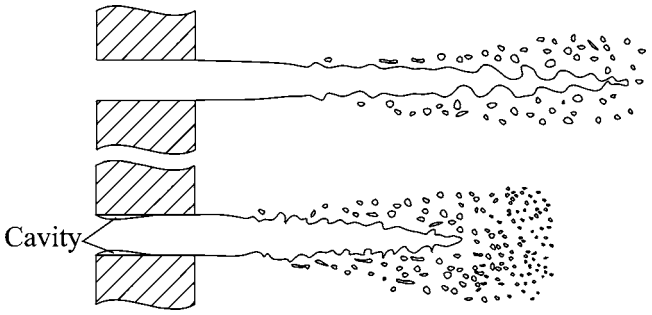

FIG. 1. The effects of cavitation on atomization of liquid jets.

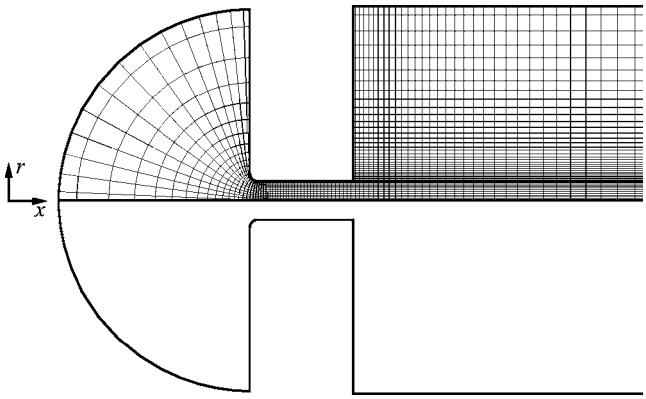

FIG. 2. Physical domain and orthogonal grid (flow from left to right).

Winer and Bair[11] and, independently, Joseph,[12] proposed that the important parameter in cavitation is the total stress which includes both the pressure and viscous stress. Kottke *et al.*[13] conducted an experiment on cavitation in creeping shear flow, where the reduction of hydrodynamic pressure does not occur. They observed the appearance of cavitation bubbles at pressures much higher than vapor pressure. Their data on cavitation inception agrees well with the total stress criterion for cavitation. Archer *et al.*[14] observed a decrease in the shear stress in the startup of steady shearing flow of a low-molecular-weight polystyrene. The decrease coincided with the opening of bubbles within the flow and occurred when the shear stress reached 0.1 Mpa.

These experiments support the idea that viscous stress plays an important role in cavitation. We wish to compare the traditional pressure criterion with the total stress criterion proposed here. It is extremely difficult to perform the comparison in experiments. The flow fields in experiments are not known in precise details; for example, low pressure can occur downstream of sharp corners. The criterion for heterogeneous cavitation cannot be known precisely since it varies from sample to sample and even varies in the corresponding sample in different experiments. These kinds of problems do not occur in the computations performed here.

Our study is meant to compare conditions for the inception of cavitation under the conventional pressure criterion and the total stress criterion. For this study, we consider flows in which no bubbles are present and their appearance is incipient. The study of the comparison of cavitation criteria in a bubble mixture is greatly more difficult and requires that one account for additional effects due to bubbly flow not considered here.

Using the total stress criterion, Funada *et al.*[15] predicted the cavitation of a two-dimensional (2D) viscous potential flow through an aperture, and Dabiri *et al.* studied the cavitation of Navier-Stokes flow in the aperture. A preliminary description of their results is given by Joseph *et al.*[16] Also, Padrino *et al.*[17] studied the cavitation predicted by total stress criterion around a sphere in a uniform flow. However, previous calculations done on the subject of high-pressure-nozzle cavitation have used the traditional criterion. The purpose of this paper is to use the new criterion to study the potential locations for the cavitation in liquid atomizers.

II. GOVERNING EQUATIONS

In this study, we consider flow of a liquid through an orifice and the exiting jet into a stagnant gas. The physical problem, the computational domain, and the grid are shown in Fig. 2. Governing equations for an unsteady, incompressible viscous flow are the Navier-Stokes equations,

$$\rho\left(\frac{\partial \mathbf{u}}{\partial t} + \mathbf{u}\cdot\nabla\mathbf{u}\right) = -\nabla p + \nabla\cdot(2\mu\mathbf{D}) + \sigma\kappa\delta(d)\mathbf{n}, \tag{1}$$

$$\mathbf{D} = \frac{1}{2}[(\nabla\mathbf{u}) + (\nabla\mathbf{u})^T], \tag{2}$$

$$\nabla\cdot\mathbf{u} = 0, \tag{3}$$

where $\mathbf{u}$ is the velocity, and ρ and μ are the fluid density and viscosity, respectively, which could be properties of either liquid or gas phase. $\mathbf{D}$ is the strain rate tensor. The last term represents the surface tension as a force concentrated on the interface. Here, σ is the surface tension coefficient, κ is the curvature of interface, δ is the Dirac delta function. d represents the distance from the interface and $\mathbf{n}$ corresponds to the unit normal vector at the interface. The flow is characterized by the density ratio of gas to liquid, viscosity ratio, and the nondimensional parameters, Reynolds number (Re) and Weber number (We), which are defined as follows:

$$\mathrm{Re} = \frac{\rho_{\mathrm{liq}} UD}{\mu_{\mathrm{liq}}}, \quad \mathrm{We} = \frac{\rho_{\mathrm{liq}} U^2 D}{\sigma}, \quad \lambda = \frac{\rho_{\mathrm{liq}}}{\rho_{\mathrm{gas}}}, \quad \eta = \frac{\mu_{\mathrm{liq}}}{\mu_{\mathrm{gas}}}. \tag{4}$$

Here, D is the orifice diameter and U is the theoretical Bernoulli velocity of the jet,

$$U = \sqrt{\frac{2(p_u - p_d)}{\rho_{\mathrm{liq}}}}, \tag{5}$$

where p_u and p_d are the far upstream and far downstream pressures, respectively.

Finding the velocity and the pressure fields, one can calculate the stress tensor using

$$\mathbf{T} = \mu[(\nabla \mathbf{u}) + (\nabla \mathbf{u})^T] - p\mathbf{I}, \tag{6}$$

where $\mathbf{I}$ is the identity matrix and superscript T refers to the transpose of a tensor. Therefore, the maximum tensile stress, T_{11} can be calculated by transforming the tensor to the diagonal form. According to the traditional pressure criterion for cavitation, cavitation will occur when the pressure drops below the critical pressure,

$$p < p_c. \tag{7}$$

The new criterion for cavitation proposed by Joseph[12] is also used to find the cavitating regions in the flow field. According to this criterion, cavitation occurs when the maximum principal stress exceeds the negative of the critical stress of liquid at the local temperature

$$T_{11} > -p_c. \tag{8}$$

The critical threshold stress, p_c, might be the vapor pressure p_v or some other appropriate value. The cavitation number, K, defines the critical stress, p_c, in a nondimensional manner,

$$K = \frac{p_u - p_d}{p_d - p_c}. \tag{9}$$

An orthogonal grid is used to discretize the domain because, in this case, many of the terms in the metric tensor will be zero and the calculation will be faster. Also, it will offer more accuracy in the calculation of the normal fluxes.

Thompson *et al.*[18] solved the two-dimensional Poisson equation with an arbitrariness in choice of source terms to generate the orthogonal coordinates. Instead of solving the 2D Poisson equations, we solve the Laplace equation corresponding to the irrotational axisymmetric flow. Therefore, potential function and stream function of the theoretical axisymmetric potential flow are used as the orthogonal-coordinates system. This choice of coordinates will increase the accuracy since the flow far from the boundaries is irrotational and thus, closely parallel to the grid. Equations for the potential ϕ and stream function ψ come from the conditions of potential flow,

$$\nabla^2 \phi = 0 \Rightarrow \frac{1}{r}\frac{\partial}{\partial r}\left(r\frac{\partial \phi}{\partial r}\right) + \frac{\partial^2 \phi}{\partial x^2} = 0, \tag{10}$$

$$\omega_\theta = 0 \Rightarrow r\frac{\partial}{\partial r}\left(\frac{1}{r}\frac{\partial \psi}{\partial r}\right) + \frac{\partial^2 \psi}{\partial x^2} = 0, \tag{11}$$

where ω_θ is the azimuthal component of vorticity. These two equations define the ϕ and ψ in the $x-r$ cylindrical coordinates. In a practical case, it is more convenient to solve the equation for x and r in the $\phi-\psi$ coordinates. The inverse form of these equations are derived as follows:

$$\frac{\partial}{\partial \phi}\left(\frac{1}{r}\frac{\partial x}{\partial \phi}\right) + \frac{\partial}{\partial \psi}\left(r\frac{\partial x}{\partial \psi}\right) = 0, \tag{12}$$

$$\frac{\partial}{\partial \phi}\left(\frac{1}{r}\frac{\partial r}{\partial \phi}\right) + \frac{\partial}{\partial \psi}\left(r\frac{\partial r}{\partial \psi}\right) = 0. \tag{13}$$

These equations are in the same format as derived by Ryskin and Leal.[19] However, they derived them for a specific choice of source terms in the 2D Poisson equations, while here, they are derived from equations of irrotational axisymmetric flow. These equations with proper boundary conditions, which come from the geometry of the boundaries and Cauchy-Riemann conditions, are solved by a second-order, finite-difference code.

III. NUMERICAL MODELING

The numerical solution of the incompressible, unsteady, axisymmetric Navier-Stokes equations is performed using the finite-volume method on a staggered grid. The convective term is discretized using the quadratic upwind interpolation for convective kinematics (QUICK) (Hayase[20]). The semi-implicit method for pressure-linked equation (SIMPLE), developed by Patankar,[21] is used to solve the pressure-velocity coupling. The time integration is accomplished using the second-order Crank-Nicolson scheme. A level-set method developed by Osher and co-workers[22,23] is used to track the interface and model the surface tension. The level-set function, denoted by θ, is defined as a signed distance function. It has positive values on one side of the interface (gas phase), and negative values on the other side (liquid phase). The magnitude of the level set at each point in the computational field is equal to the distance from that point to the closest point on the interface.

The level-set function is being convected by the flow as a passive scalar variable,

$$\frac{\partial \theta}{\partial t} + \mathbf{u} \cdot \nabla \theta = 0. \tag{14}$$

It is obvious that, if the initial distribution of the level set is a signed distance function, after a finite time of being convected by a nonuniform velocity field, it will not remain a distance function. Therefore, we need to reinitialize the level-set function so it will be a distance function (with property of $|\nabla \theta| = 1$) without changing the zero level set (position of the interface).

Suppose $\theta_0(\mathbf{x})$ is the level-set distribution after some time step and is not exactly a distance function. This can be reinitialized to a distance function by solving the following partial differential equation:[22]

$$\frac{\partial \theta'}{\partial \tau} = \text{sign}(\theta_0)(1 - |\nabla \theta'|), \tag{15}$$

with initial conditions,

$$\theta'(\mathbf{x}, 0) = \theta_0(\mathbf{x}),$$

where

$$\text{sign}(\theta) = \begin{cases} -1 & \text{if } \theta < 0 \\ 0 & \text{if } \theta = 0 \\ 1 & \text{if } \theta > 0 \end{cases} \tag{16}$$

and τ is a pseudotime. The steady solution of Eq. (15) is the distance function with property $|\nabla \theta| = 1$, and since sign(0) $= 0$, then θ' has the same zero level set as θ_0.

Now using the level-set definition, the fluid properties can be defined as

$$\rho = \rho_{\text{liq}} + (\rho_{\text{gas}} - \rho_{\text{liq}})H_\epsilon(\theta), \tag{17}$$

$$\mu = \mu_{\text{liq}} + (\mu_{\text{gas}} - \mu_{\text{liq}})H_\epsilon(\theta), \tag{18}$$

where H_ϵ is a Heaviside function that has a continuous jump,

$$H_\epsilon = \begin{cases} 0 & \theta < -\epsilon, \\ (\theta+\epsilon)/(2\epsilon) + \sin(\pi\theta/\epsilon)/(2\pi) & |\theta| \leqslant \epsilon, \\ 1 & \theta > \epsilon, \end{cases} \tag{19}$$

where ϵ represents the thickness of the interface and has the value of $1.5h$, where h is the cell size. This Heaviside function corresponds to a delta function that can be used to evaluate the force caused by surface tension,

$$\delta_\epsilon = \begin{cases} [1+\cos(\pi\theta/\epsilon)]/(2\epsilon) & |\theta| \leqslant \epsilon, \\ 0 & \text{otherwise}. \end{cases} \tag{20}$$

The last term in the momentum equation (1) includes the normal unity vector and the curvature of the interface which can be calculated as follows:

$$\mathbf{n} = \frac{\nabla\theta}{|\nabla\theta|}, \quad \kappa = -\nabla\cdot\mathbf{n}. \tag{21}$$

IV. RESULTS

The computational domain is shown in Fig. 2. The calculation is done for Reynolds numbers equal to 100, 200, 500, 1000, and 2000. Upstream and downstream boundaries are at distance of 5 diam from the orifice. Pressure boundary conditions are applied on both upstream and downstream boundaries. On the downstream boundary, the Lagrangian time derivative of velocities is set to zero. The grid independency of the solution was investigated for flow with Re =2000, by increasing the number of grid points by 50%. The maximum change in the velocity profile at the exit of the nozzle was less than 0.5%. Also, the independency of the solution to the size of the domain is verified. For flow with the Re=100 and the domain was extended by 50%, the maximum change in the velocity profile at the exit was about 0.1%.

The value of the discharge coefficient and its dependence on the Reynolds number are determined and compared to results by Payri *et al.*,[24] who have conducted an experiment on the diesel fuel injectors. Discharge coefficient is defined as the ratio of average velocity in the nozzle to the ideal Bernoulli velocity,

$$C_d = \frac{U_{\text{ave}}}{U} = \frac{\dot{m}}{A\sqrt{2\rho(P_u - P_d)}}, \tag{22}$$

where $\dot{m}$ is the mass flux and A is the cross-sectional area of the orifice.

These results are shown in Fig. 3. The difference between this calculation and the experiment is less than 4%, while the uncertainty of the experimental results is reported as 2.5%. Experimental results show a slightly lower discharge coefficient, which could be due to pressure loss in parts before the orifice. In these calculations, the Reynolds number is based on the average velocity of flow in the nozzle used in the experiment.

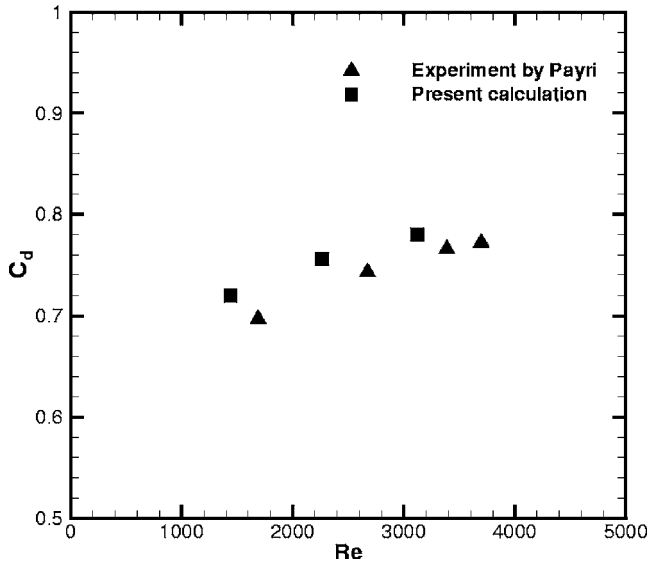

FIG. 3. Discharge coefficient of the orifice for different Reynolds numbers, compared with experiments by Payri *et al.* (Ref. 24).

A. Effect of Reynolds number on cavitation

In this section, the axisymmetric flow in a fixed geometry with various Reynolds numbers is studied. Liquid-to-gas density ratio and viscosity ratio are $\lambda=100$ and $\eta=10$, respectively, and the Weber number is We=1000, while Reynolds number varies between 100 and 2000. The length-to-diameter ratio of the orifice is $L/D=2$ and the inlet corner is rounded with radius of $R/D=0.02$. However, the outlet corner is sharp.

After several residence time the flow reaches a steady state. It has been observed[25,26] that the unsteadiness due to Kelvin-Helmholtz or Rayleigh instability will be observable at distances of more than 20 diam downstream of the orifice. Therefore, in this study we expect to have steady flow everywhere.

For Reynolds number Re=100, Fig. 4 shows the velocity profiles and normalized pressure distribution. The liquid-gas interface leaving the downstream corner is also shown. The flow has an almost fully developed parabolic profile at the exit and there is no separation at the upstream corner. A small contraction can be seen in the liquid jet after leaving the orifice.

The flow for Re=2000 is shown in Fig. 5. The pressure has a minimum at the upstream corner, where the cavitation is likely to occur. Note that the exit velocity profile indicates a boundary layer but full development has not occurred. At the upstream curved corner the flow separates from the wall and reattaches to the wall further downstream and creates a recirculating region. The recirculating region is shown in Fig. 5. The recirculating region will grow as the Reynolds number increases.

In the following part the two criteria for predicting the cavitation are compared. Note that the flow inside the nozzle

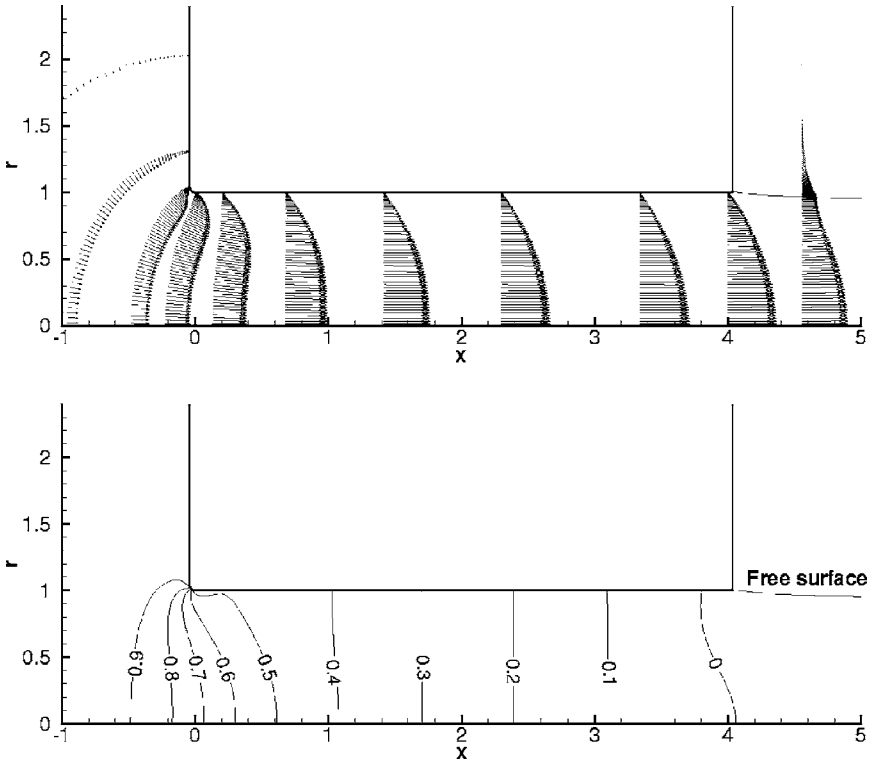

FIG. 4. Velocity profiles and contours of $(p-p_d)/\frac{1}{2}\rho U^2$ for flow with Re $=100$.

is considered to be single phase (liquid) only, and the regions at risk of cavitation, i.e., regions in which the cavitation criterion is satisfied, are specified. For flows with different Reynolds numbers, the total stress is calculated in the flow field, and regions where the cavitation occurs based on each criterion are identified. In each plot, the curves in which cavitation is likely to occur is plotted for the same flow parameters but different values of cavitation number, K, corresponding to different critical stresses. Figure 6 shows these vulnerable regions for Re$=200$ and Re$=500$. At Reynolds number of 200, for flow with $K=10$, the use of the pressure criterion predicts almost no cavitation in the flow, while the use of the total stress predicts a larger domain of cavitation. This could be explained by the fact that in the lower Reynolds number the viscous stress is stronger and there will be a larger difference between pressure and total stress.

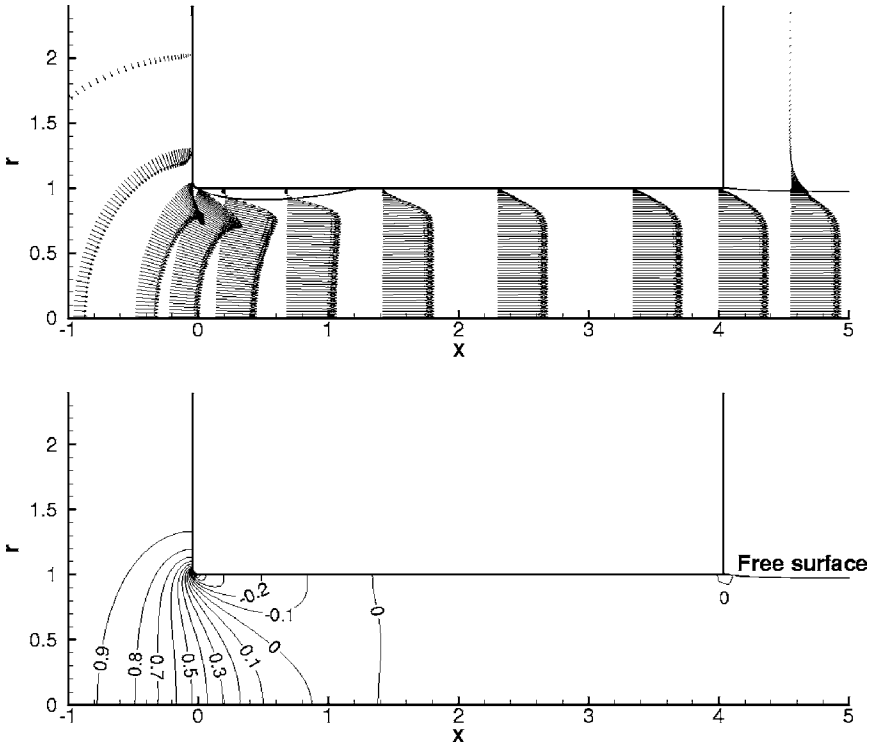

FIG. 5. Velocity profiles and contours of $(p-p_d)/\frac{1}{2}\rho U^2$ for flow with Re $=2000$.

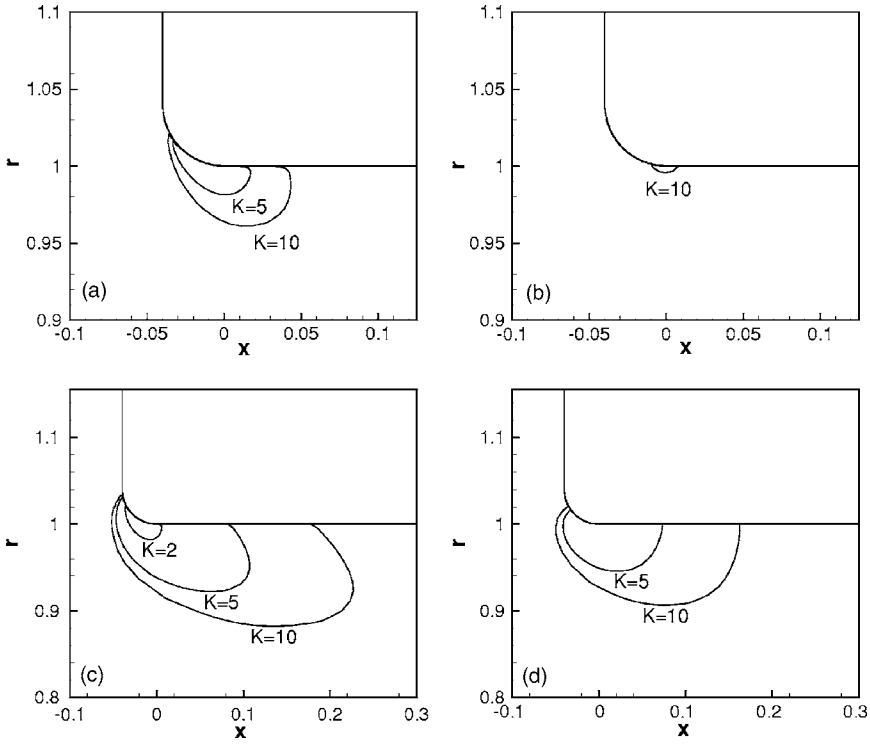

FIG. 6. The cavitation threshold curves on which $T_{11}+p_c=0$ in different flows with $K=2,5,10$. We=1000, $L/D=1$. (a) Re=200, total stress criterion; (b) Re=200, pressure criterion; (c) Re=500, total stress criterion; (d) Re=500, pressure criterion.

Flows with Re=1000 and Re=2000 are shown in Fig. 7. For higher Reynolds numbers the difference between two criteria becomes less, but still the cavitating region predicted by the total-stress criterion stretches further downstream. This stretching appears at a short distance from the orifice wall. It occurs in the high-shear-stress region inside the separated boundary layer. Note that the plots in Figs. 6 and 7 have different scales. Figure 8 shows the thresholds values of K above which the cavitation will be present inside the nozzle based on both pressure and total-stress criteria for different values of length-to-diameter ratios. Apparently, the total-stress criterion predicts more chances of cavitation than the pressure criterion. The relative difference between two criteria is larger at lower Reynolds numbers but decreases as the Reynolds number increases. At Re=2000, which is close to some practical situations, the relative difference between

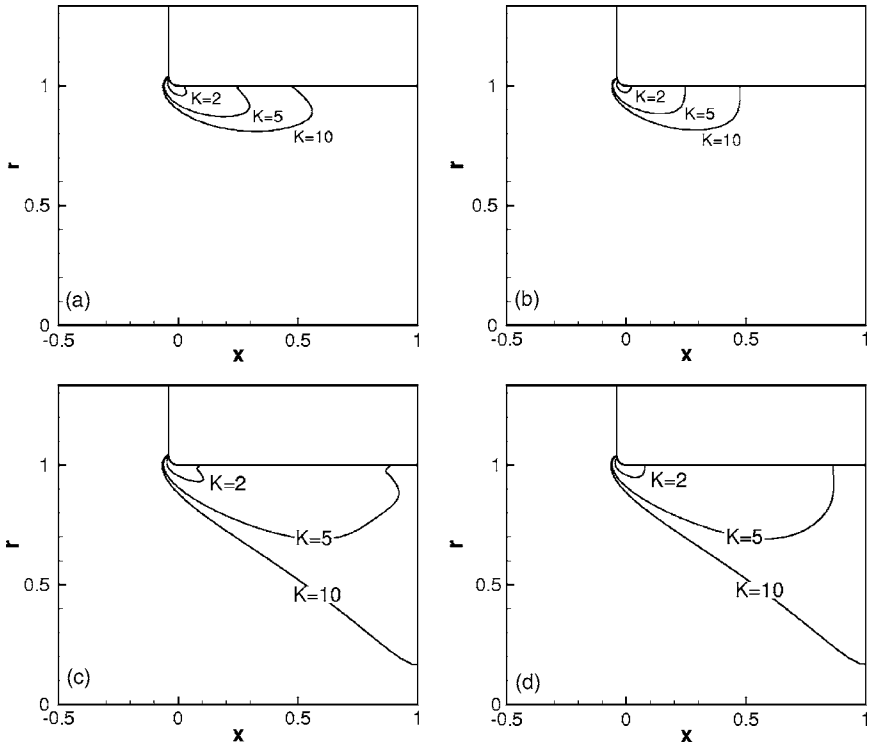

FIG. 7. The cavitation threshold curves on which $T_{11}+p_c=0$ in different flows with $K=2,5,10$. We=1000, $L/D=1$. (a) Re=1000, total stress criterion; (b) Re=1000, pressure criterion; (c) Re=2000, total stress criterion; (d) Re=2000, pressure criterion.

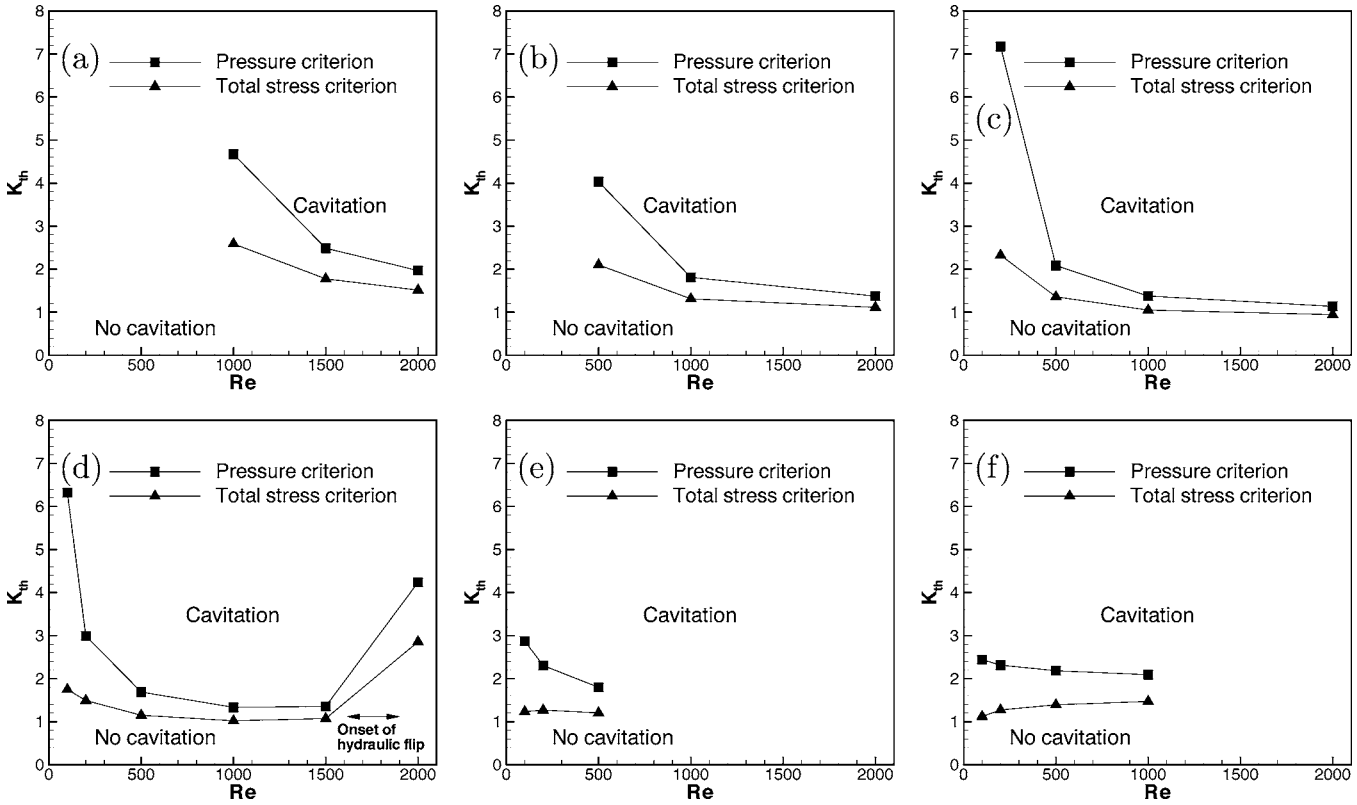

FIG. 8. Threshold values of K above which cavitation occurs in the orifice. L/D= 5 (a), 2 (b), 1 (c), 0.5 (d), 0.2 (e), and 0.1 (f).

the threshold value of K predicted by two criteria is about 20%, 23%, and 30% for length-to-diameter ratios of one, two, and five, respectively.

Although the existence of cavitation bubbles would change the flow field downstream of the inception point, the analysis is helpful to understand the significance of viscous stress in the cavitation inception. Therefore, the predicted region of cavitation might not be quantitatively accurate because of the effects of bubbles, but the plot of the threshold value of the cavitation number based on Reynolds number is accurate and will not be affected by the presence of bubbles, since it is the condition at which the flow starts to cavitate, and one can approach this point from a noncavitating flow.

Going to lower length-to-diameter ratios, two interesting things happen. The first is the hydraulic flip, which is discussed in Sec. IV C. The second phenomenon is that, for a length-to-diameter ratio of L/D=0.1, the trend of K based on total-stress criterion versus Reynolds number changes and it increases as Reynolds number increases. This means less chance of cavitation for higher Reynolds numbers and agrees with the statement by Padrino *et al.*[17] about the increase in risk of cavitation for more viscous fluids.

B. Effects of curvature of inlet corner

According to the inviscid theory, both the pressure and the strain rate become unbounded at convex sharp corners. However, in real situations, because of the existence of boundary layer and no-slip condition, and also separation of flow at sharp corners, all parameters remain finite. But still it is expected that the behavior of the flow will be very dependent on the geometry of the corner. Here we will look at flows in nozzles with different radii of curvature at the inlet corner. R/D is varied between 0.01 and 0.04 while keeping other parameters of the flow and domain constant. Figure 9 shows the threshold value of K vs R/D. For both Reynolds numbers of 1000 and 2000, the K_{th} increases as the R/D increases. This is expected because the larger the radius of curvature, the smaller the increase in velocity and drop in pressure.

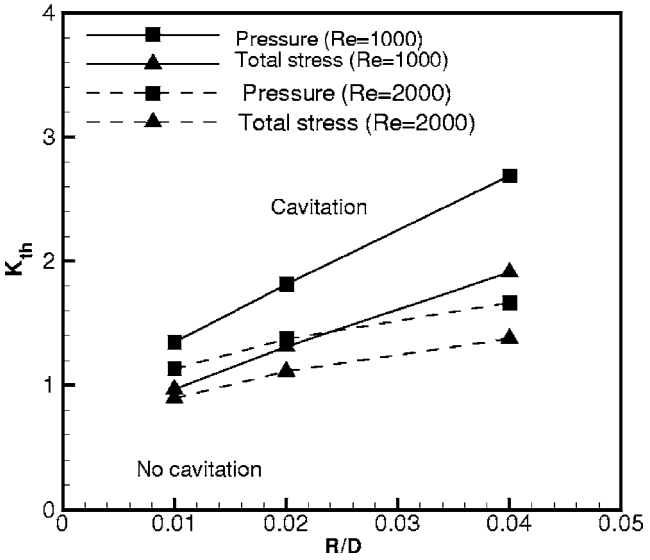

FIG. 9. Threshold values of K above which cavitation occurs in the orifice, predicted by pressure and total stress criteria for L/D=2, Re=1000, 2000.

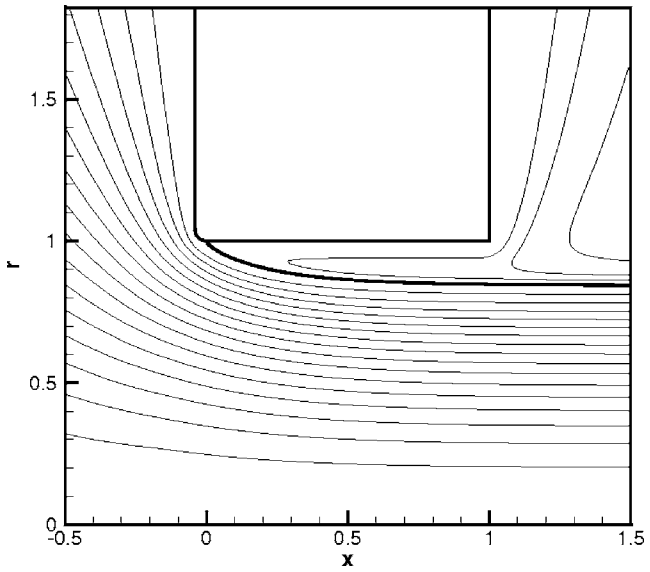

FIG. 10. Streamlines for flow with Re=2000, $L/D=0.5$

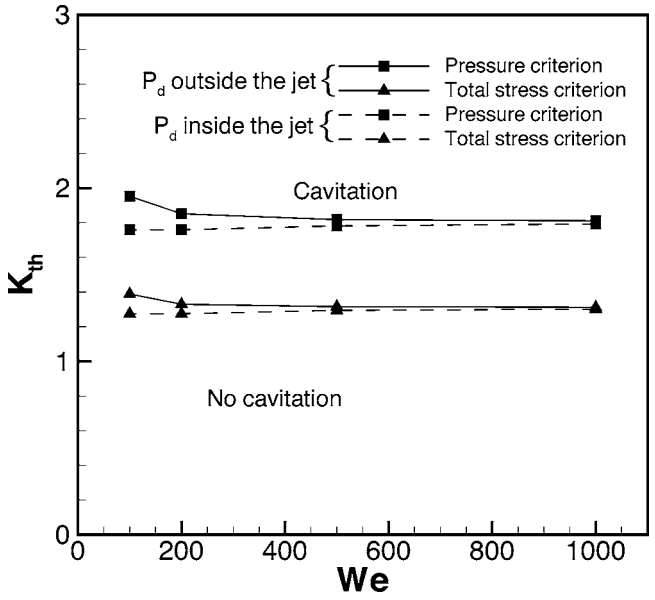

FIG. 11. Threshold values of K for which cavitation occurs in the orifice for Re=1000, $L/D=2.0$, and different Weber numbers.

C. Hydraulic flip and its effects on cavitation

It has been seen that for Reynolds number of 1000 and above flow separates from the wall of the nozzle at the upstream curved corner. This separation creates a recirculation region, which extends downstream of the orifice as Reynolds number increases. If this recirculation reaches the downstream corner, then it will merge with the entrained flow outside of the orifice, causing the air to enter the orifice and fill the recirculating region.

In order to observe this phenomenon we need higher Reynolds numbers or shorter nozzles. For a diameter-to-length ratio of 0.5, the hydraulic flip happens between Reynolds numbers of 1500 and 2000. The streamlines for the flow with Re=2000 are shown in Fig. 10. The thicker line is the liquid-gas interface. Since the flow inside the nozzle reaches a steady state, the streamlines and material lines will be the same and the interface will be a streamline as well. The threshold value of K for this geometry is shown in Fig. 8(d). The behavior of threshold value of K versus Reynolds number is similar to the results for lower Reynolds number, i.e., K decreases as Reynolds number increases and the total stress criterion predicts a smaller K. However, for Reynolds number of 2000, where hydraulic flip happens, the value of K jumps to a higher value, which indicates that the cavitation has less chance to occur. This phenomenon has been observed in experiments as well,[3,27] and could be explained by the fact that the air entering the recirculating region will keep the pressure close to downstream pressure.

D. Effect of Weber number on cavitation

Effect of the Weber number on the cavitation is studied for the flow with Reynolds number of 1000 and orifice with length-to-diameter ratio of two. Threshold values of cavitation number are plotted in Fig. 11 for Weber numbers of 100, 200, 500, and 1000. As it can be seen in Fig. 11, the threshold value of K is almost constant for Weber numbers of 500 and above and increases as the Weber number decreases. This could be explained as a consequence of higher pressure difference, for lower Weber number, applied by the surface tension to the liquid inside the jet and the nozzle. Dashed lines in Fig. 11 show that there is no Weber number effect if we use downstream exit pressure in the liquid and do not consider the capillary pressure. The effect of surface tension for We$>$500 is insignificant for the internal flow and near downstream jet; it probably becomes more significant further downstream.

V. CONCLUSIONS

The viscous incompressible axisymmetric flow of a liquid through an orifice has been simulated in order to compare the cavitation predicted by the pressure criterion and the total-stress criterion. The total-stress criterion predicts larger cavitating regions in the flow field and also a lower threshold value of K, cavitation number, for occurrence of cavitation relative to the pressure criterion. The hydraulic flip phenomenon is also observed for flows with high Reynolds number through orifices with small length-to-diameter ratios. It has been observed that when hydraulic flip occurs, the cavitating region will shrink or even disappear, which is in agreement with experimental observations.

ACKNOWLEDGMENT

This research has been supported by the U.S. Army Research Office through Grant/Contract No. W911NF-06-1-0225, with Dr. Kevin McNesby and Dr. Ralph Anthenien having served sequentially as program managers.

[1] N. Tamaki, M. Shimizu, K. Nishida, and H. Hiroyasu, "Effects of cavitation and internal flow on atomization of a liquid jet," Atomization Sprays **8**, 179 (1998).
[2] N. Tamaki, M. Shimizu, and H. Hiroyasu, "Enhancement of the atomization of a liquid jet by cavitation in a nozzle hole," Atomization Sprays **11**, 125 (2001).
[3] H. Hiroyasu, "Spray breakup mechanism from the hole-type nozzle and its

applications," Atomization Sprays **10**, 511 (2000).
[4]M. Otendal, O. Hemberg, T. T. Tuohimaa, and H. M. Hertz, "Microscopic high-speed liquid-metal jets in vacuum," Exp. Fluids **39**, 799 (2005).
[5]R. A. Bunnell, S. D. Heister, C. Yen, and S. H. Collicott, "Cavitating injector flows: Validation of numerical models and simulations of pressure atomizers," Atomization Sprays **9**, 445 (1999).
[6]H. Tafreshi and B. Pourdeyhimi, "Simulating cavitation and hydraulic flip inside hydroentangling nozzles," Text. Res. J. **74**, 359 (2004).
[7]K. Ahn, J. Kim, and Y. Yoon, "Effects of orifice internal flow on transverse injection into subsonic crossflows: Cavitation and hydraulic flip," Atomization Sprays **16**, 15 (2006).
[8]K. Jung, T. Khil, and Y. Yoon, "Effects of orifice internal flow on breakup characteristics of like-doublet injectors," J. Propul. Power **22**, 653 (2006).
[9]L. C. Ganippa, G. Bark, S. Andersson, and J. Chomiak, "Cavitation: a contributory factor in the transition from symmetric to asymmetric jets in cross-flow nozzles," Exp. Fluids **36**, 627 (2004).
[10]C. E. Brennen, *Cavitation and Bubble Dynamics* (Oxford University Press, New York, 1995).
[11]S. Bair and W. O. Winer, "The high-pressure high shear-stress rheology of liquid lubricants," Trans. ASME, J. Tribol. **114**, 1 (1992).
[12]D. D. Joseph, "Cavitation and the state of stress in a flowing liquid," J. Fluid Mech. **366**, 367 (1998).
[13]P. A. Kottke, S. S. Bair, and W. O. Winer, "Cavitation in creeping shear flows," AIChE J. **51**, 2150 (2005).
[14]L. A. Archer, D. Ternet, and R. G. Larson, "'Fracture' phenomena in shearing flow of viscous liquids," Rheol. Acta **36**, 579 (1997).
[15]T. Funada, J. Wang, and D. D. Joseph, "Viscous potential flow analysis of stress induced cavitation in an aperture flow," Atomization Sprays **16**, 763 (2006).
[16]D. D. Joseph, T. Funada, and J. Wang, *Potential Flows of Viscous and Viscoelastic Fluids* (Cambridge University Press, Cambridge, UK, in press), p. 287.
[17]J. C. Padrino, D. D. Joseph, T. Funada, J. Wang, and W. A. Sirignano, "Stress-induced cavitation for the streaming motion of a viscous liquid past a sphere," J. Fluid Mech. **578**, 381 (2007).
[18]J. F. Thompson, F. C. Thames, and C. W. Mastin, "Automatic numerical generation of body-fitted curvilinear coordinate system for field containing any number of arbitrary 2-dimensional bodies," J. Comput. Phys. **15**, 299 (1974).
[19]G. Ryskin and L. Leal, "Orthogonal mapping," J. Comput. Phys. **50**, 71 (1983).
[20]T. Hayase, J. A. C. Humphrey, and R. Greif, "A consistently formulated quick scheme for fast and stable convergence using finite-volume iterative calculation procedure," J. Comput. Phys. **98**, 108 (1992).
[21]S. V. Patankar, *Numerical Heat Transfer and Fluid Flow* (Hemisphere, Washington, DC, 1980).
[22]M. Sussman, E. Fatemi, P. Smereka, and S. Osher, "An improved level set method for incompressible two-phase flows," Comput. Fluids **27**, 663 (1998).
[23]S. Osher and R. P. Fedkiw, "Level set methods: an overview and some recent results," J. Comput. Phys. **169**, 436 (2001).
[24]F. Payri, V. Bermudez, R. Payri, and F. J. Salvador, "The influence of cavitation on the internal flow and the spray characteristics in diesel injection nozzles," Fuel **83**, 419 (2004).
[25]Y. Pan and K. Suga, "A numerical study on the breakup process of laminar liquid jets into a gas," Phys. Fluids **18**, 052101 (2006).
[26]J. H. Rupe, "On the dynamic characteristics of free liquid jets and a partial correlation with orifice geometry," NASA Technical Report No. JPL-TR-32-207 (1962).
[27]H. Chaves, M. Knapp, A. Kubitzek, F. Obermeier, and T. Schneider, "Experimental study of cavitation in the nozzle hole of diesel injectors using transparent nozzles," SAE Paper No. 950290 (1995).